BMC Medical Imaging

RESEARCH Open Access

The value of multiparametric MRI radiomics and machine learning in predicting preoperative Ki-67 expression level in breast cancer

Yan Lu[1†], Long Jin[1†], Ning Ding[1*], Mengjuan Li[1], Shengnan Yin[1] and Yiding Ji[1]

Abstract

Objective This study was to develop a multi-parametric MRI radiomics model to predict preoperative Ki-67 status.

Materials and methods A total of 120 patients with pathologically confirmed breast cancer were retrospectively enrolled and randomly divided into a training set ($n=84$) and a validation set ($n=36$). Radiomic features were derived from both the intratumoral and peritumoral regions, extending 5 mm from the tumor boundary, using magnetic resonance imaging (MRI). The MRI sequences employed included T2-weighted imaging (T2WI), dynamic contrast-enhanced (DCE) imaging, diffusion-weighted imaging (DWI), and apparent diffusion coefficient (ADC) maps. The T-test and the Least Absolute Shrinkage and Selection Operator Cross-Validation (LASSO CV) were conducted for feature selection. $Model_{intra}$, $model_{peri}$, $model_{intra+peri}$ were established by eleven supervised machine learning (ML) algorithms to predict the expression status of Ki-67 in breast cancer and were verified by the validation groups. The model's performance was evaluated by employing metrics such as the area under the curve (AUC), accuracy, sensitivity, and specificity.

Results The features of intratumor, peritumor, intratumor + peritumor were extracted 851, 851 and 1702 samples respectively, 14, 23 and 35 features were selected by LASSO. ML algorithms based on $model_{intra}$ and $model_{peri}$ consistently yield AUCs that are below 80% in the validation set. Hower, Logistic regression (LR) and linear discriminant analysis (LDA) based on $model_{intra+peri}$ demonstrated significant advantages over other algorithms, achieving AUCs of 0.92 and 0.98, accuracies of 0.94 and 0.97, sensitivities of 1 and 0.96, and specificities of 0.85 and 1 respectively in the validation set.

Conclusion The integrated intra- and peritumoral radiomics model, developed using multiparametric MRI data and machine learning classifiers, exhibits significant predictive power for Ki-67 expression levels. This model could facilitate personalized clinical treatment strategies for individuals diagnosed with breast cancer (BC).

Clinical trial number Not applicable.

[†]Yan Lu and Long Jin contributed equally to this work.

*Correspondence:
Ning Ding
1102799081@qq.com

Full list of author information is available at the end of the article

Keywords Radiomics, Machine learning, Breast cancer, Ki-67 expression level

Introduction

Breast cancer (BC) constitutes the highest incidence worldwide, as the commonest malignant cancer in women globally [1, 2]. Based on precision medicine, tumor biomarkers including Ki-67 protein are becoming more and more important in clinical research. Ki-67 is correlated with tumor invasion, risk of recurrence, and prognosis, serving as a significant prognostic indicator. and has been used for individualized treatment for breast cancer [3–6].

Immunohistochemistry (IHC) has become the primary method for evaluating preoperative Ki-67 expression levels. Nevertheless, it is invasive and may pose a risk of complications. Sampling error may exist in biopsy because of heterogeneity in tumor [7].Because the expression level of Ki-67 changes dynamically, detection of Ki-67 through postoperative biopsy cannot accurately guide clinical treatment prior to surgery. Studies have found high Ki-67 expression in breast cancer patients with pathological complete response (pCR), and preoperative Ki-67 status was beneficial to patients receiving neoadjuvant chemotherapy (NAC) in predicting pCR [8, 9]. Additionally, Ki-67 was approved for predicting the recurrence-free survival rate in patients receiving short-term endocrine therapy [10]. Therefore, it is essential to identify a timely and noninvasive approach for the preoperative detection of Ki-67 expression status.

Radiomics is a rapidly emerging technology. It involves the high-throughput extraction of quantitative features from medical images [11, 12]. These visually unidentifiable information can be used to develop machine learning (ML) models for clinical prediction [13]. Radiomics with magnetic resonance imaging (MRI) can be used to discriminate molecular subtype, predict human epidermal growth factor receptor-2 (HER-2) and Ki-67 status, identify lymph node metastasis in patients with BC [14–18]. Cui et al. [19] showed that the AUC values is 0.78 and 0.71 respectively of the model predicting positive expression of Ki-67 and P53. However, the acquired image features by ultrasonic can easily be affected by operator experience. Li et al. [17]reported that radiomics signatures extracted from dynamic contrast-enhanced MRI (DCE-MRI) had the potential to identify HER-2 and Ki-67 status. Previous studies mostly focused on single MRI sequence, which may be insufficient to evaluate pictorial information. Liu et al. [20] conducted deep learning by extracting radiomics from T2-weighted imaging (T2WI), diffusion-weighted imaging (DWI), and DCE-MRI, they found that a multi-parameter classification model has better predictive ability for Ki-67 compared to models with single sequence. However, this study only extracted radiomics features of part regions in the lesion area without three-dimensional structure.

The study aimed to assess the accuracy of radiomics ML model based on combined intra- and peritumoral regions in functional multi-parameter MRI (mp-MRI) maps in prediction of Ki-67 expression level in patients with BC.

Materials and methods

Patient population

A total of 145 female patients diagnosed with invasive ductal carcinoma between January 2019 and November 2022 were retrospectively enrolled. Inclusion criteria: (1) Breast cancer confirmed by histopathology with Ki-67 detection. (2) Breast MRI examination was performed 1 week before treatment. (3) Patients without other primary tumors. Exclusion criteria: (1) Image quality were poor. (2) Patients were treated with radiotherapy or chemotherapy before MR examination. 120 targets were finally enrolled (72 with Ki-67 high expression and 48 with Ki-67 low expression) and were randomly assigned into the training and validation cohorts at a ratio of 7:3. The age range is from 32 to 77 years old, with an average age of 55.78±8.94 years. Table 1 listed the clinical information of patients.

Pathological assessment

IHC was used to determine the expression of ER(estrogen receptor, ER), PR(progesterone receptor, PR), HER-2, and Ki-67. Ki-67 was considered high if the Ki-67 level was greater than 14%. Tumors with staining intensity scores of 3+were considered as positive HER-2 status.

MRI examination

All MR examinations were conducted using a 3.0 T magnetic resonance scanner (Magnetom Verio, Siemens, Germany) equipped with an 8-channel breast phased-array coil. Several standard imaging sequences were involved: (1)T2WI, repetition time (TR): 3380 ms, time to echo (TE): 61 ms, slice thickness: 4.0 mm, 0.8 mm slice interval, field of view (FOV) 340*340 mm; matrix 320*192 mm; (2) DWI, TR 5500 ms, TE 5 ms, acquisition frequency 2442 Hz/pixel, slice thickness 5 mm, 1.0 mm slice interval, diffusion sensitivity coefficient b=800s/mm^2, FOV 340*349 mm; matrix 130*96 mm; (3) ADC diagram was generated automatically; (4) DCE, TR 4.67 ms, TE 1.66 ms, slice thickness 1.2 mm, 0 slice interval, FOV 340*340 mm; matrix 448*336 mm.

Table 1 MRI morphologic features and clinical and histopathological characteristics of IBC patients in the training and validation cohorts

Characteristics	Training cohort($n=84$)			Validation cohort($n=36$)		
	High Ki−67($n=49$)	Low Ki−67($n=35$)	*p*	High Ki−67($n=23$)	Low Ki−67($n=13$)	*p*
Age (mean ± SD)	55.94 ± 8.12	56.29 ± 9.08	0.340	54.70 ± 9.89	55.69 ± 10.66	0.517
Menopausal status			0.795			0.878
Premenopausal	21(42.9%)	14(40%)		13(56.5%)	7(53.8%)	
Postmenopausal	28(57.1%)	21(60%)		10(43.5%)	6(46.2%)	
Lesion type			0.473			0.683
Mass	39(79.6%)	30(85.7%)		19(82.6%)	10(76.9%)	
Non-mass enhancement	10(20.4%)	5(14.3%)		4(17.4%)	3(23.1%)	
Lesion internal enhancement			0.004			0.555
Homogeneous	21(42.9%)	26(74.3%)		10(43.5%)	7(53.8%)	
Heterogeneous	28(57.1%)	9(25.7%)		13(56.5%)	6(46.2%)	
Mass shape*			0.612			0.340
Round or oval	21(53.8%)	18(60%)		13(68.4%)	5(50%)	
Irregular	18(46.2%)	12(40%)		6(31.6%)	5(50%)	
Mass margin*			0.488			0.948
Circumscribed	29(74.4%)	20(66.7%)		15(78.9%)	8(80%)	
Irregular or speculated	10(25.6%)	10(33.3%)		4(21.1%)	2(20%)	
Tumor grade			0.106			0.772
II	22(44.9%)	22(62.9%)		13(56.5%)	8(61.5%)	
III	27(55.1%)	13(37.1%)		10(43.5%)	5(38.5%)	
HER-2			0.019			0.592
Positive	22(44.9%)	28(80%)		11(47.8%)	5(38.5%)	
Negative	27(55.1%)	7(20%)		12(52.2%)	8(61.5%)	
ER			< 0.001			0.027
Positive	26(53.1%)	3(8.6%)		13(56.5%)	12(92.3%)	
Negative	23(46.9%)	32(91.4%)		10(43.4%)	1(7.7%)	
PR			< 0.001			0.143
Positive	22(44.9%)	5(14.3%)		10(43.4%)	8(66.7%)	
Negative	27(55.1%)	30(85.7%)		13(56.5%)	4(33.3%)	

* Mass shape and margin were calculated with a denominator of 69 masses in the training cohort and 29 in the validation cohort. Data are numbers of patients, with percentages in parentheses. IBC, invasive breast cancer; SD, standard deviation; HER2, human epidermal growth factor receptor 2; ER, estrogen receptor; PR, progesterone receptor

MRI image analysis

Two radiologists were arranged to retrospectively analyze MRI images. Both radiologists were blinded to the pathological outcomes. They assessed the morphologic features of masses containing lesion type, shape, margin and internal enhancement [21]. Another radiologist with 20 years of experience was consulted in case of disagreements.

Lesion delineation and segmentation

Images from sequences of the second post-contrast images of DCE, T2WI, DWI_{b800} and ADC were exported from the picture archiving and communication system (PACS) into 3D Slicer software (https://www.slicer.org/) . A radiologist with 5 years of experience manually and volumetrically segmented the regions of interest (ROI). The ROIs were reviewed by another experienced radiologist. They were all blinded to clinical and pathological information. ROI delineation was contoured along the margin of each slice of the tumor. The ROI on ADC maps was transferred from DWI maps. The peritumoral regions were obtained automatically from intratumoral regions by 3D Slicer software. The distance of equidistant 3-dimensional dilation was 5 mm. The overview of research process was shown in Fig. 1.

Radiomic feature extraction

A total of 851, 851 and 1702 radiomics characteristics were calculated using the Pyradiomics package (https://www.radiomics.io/pyradiomics.html) extracted from intratumor, peritumor, intratumor+peritumor ROIs. Characteristics contained first-order statistical features ($n=18$) such as mean and peak value, shape-based features ($n=14$), texture features ($n=75$) such as Gray Level Dependence Matrix, Gray Level Neighborhood Matrix and wavelet features ($n=744$).

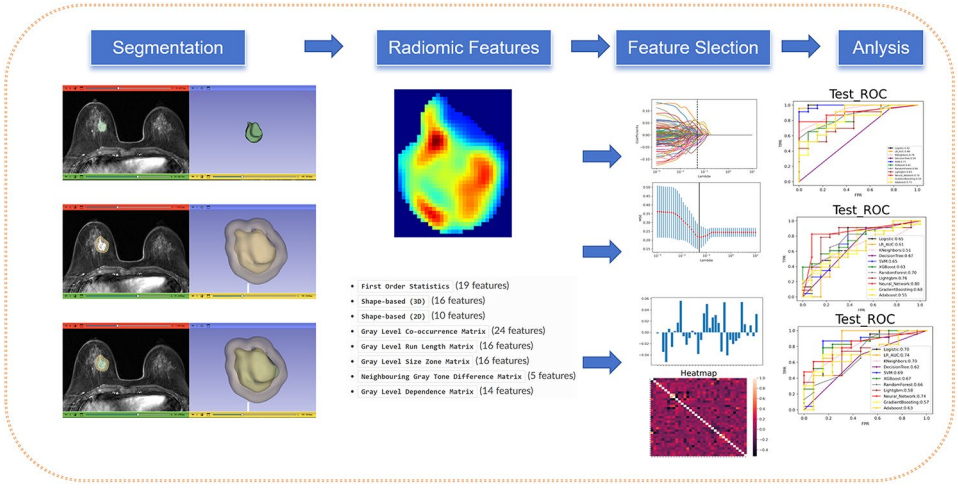

Fig. 1 An overview of the study methodology

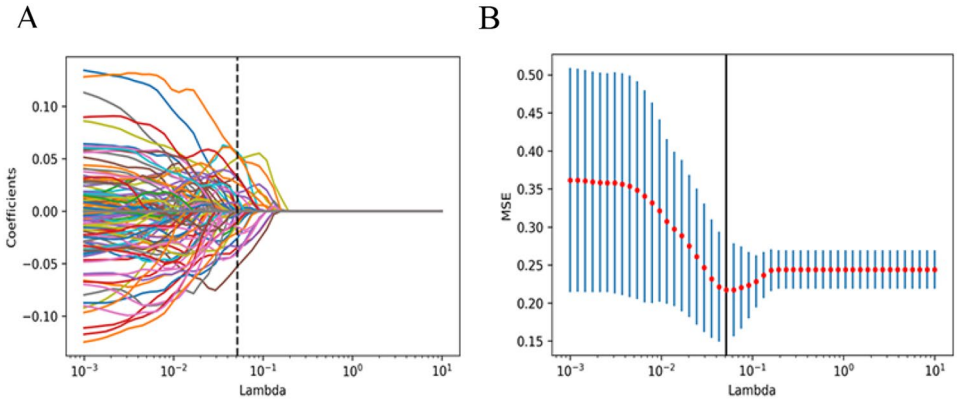

Fig. 2 Intratumoral combined with peritumoral Radiomics features were selected using the Least absolute shrinkage and selection operator cross validation (LASSO CV) method, as shown in Fig. 2A and B. The LASSO regression method was used for feature selection according to leave-one-out cross-validation (**A**), and the optimal number of features for prediction was determined based on the lowest misclassification error (**B**). These radiomics signatures were developed for predicting pathway alterations

Feature selection and radiomic model construction

The T-test and the Least absolute shrinkage and selection operator cross-validation (LASSO CV) were used for filtering the most relevant features in training group (Fig. 2). 14, 23 and 35 features were selected from intratumor, peritumor, intratumor+peritumor ROIs. 17 peritumoral features (out of 35) included in the modelintra+peri. $Model_{intra}$, $model_{peri}$, $model_{intra+peri}$ were established by eleven supervised machine learning (ML). Algorithms consisted Support Vector Machine (SVM)), Logistic Regression (LR), Decision Tree (DT), Linear Discriminant Analysis (LDA), Adaptive Boosting (AdaBoost) and so on. The radiomics ML models were evaluated using 10-fold cross-validation five times, average values of scores of models obtained were taken for evaluation. The models were independently verified in the validation cohort using area under the receiver operating characteristic (ROC) curve (AUC), accuracy, sensitivity, specificity, and F-1 score as metrics. These metrics were calculated by Anaconda software (https://www.anaconda.com/).

Statistical analysis

Descriptive data and continuous variables were assessed by independent sample t-test, categorical variables was analyzed by chi-square test on SPSS 17.0. The probability (P) value of <0.05 represents statistically significant. Univariate analysis of selected features and correlation analysis were used by the Mann-Whitney U test and Spearman rank correlation test. The measurement of AUC, sensitivity and specificity were compared by Python 3.9 (https://www.python.org/) [22].

Results

Clinical characteristics

The clinical characteristics of all patients are listed in Table 1. Lesion internal enhancement, HER-2, ER, PR, status varied significantly between the high Ki-67 and

low Ki-67 groups (with $P<0.05$) in the training cohort, and ER status varied significantly validation. There exists no significant difference in age, menopausal status, lesion type, mass shape and tumor grade($P>0.05$).

Radiomics features

The Correlation matrix of variables (Fig. 3A) showed that optimal features from the combined intra and peritumoral regions are relatively independent. Features selected were correlated with Ki-67 expression status(Fig. 3B). The details of 35 radiomics features identified were presented in Table 2.

The predictive performance of radiomics models

Features selected from the intra-tumor group, peritumor group, and intra-tumor+peri-tumor group were used to build prediction models with 11 ML algorithms. Area under the curve(AUC) values comparison was shown in Fig. 4. AUC values of different ML algorithms based on $model_{intra+peri}$ for identification of Ki-67 status in the training and testing cohort (Fig. 4A); AUC values of different ML algorithms based on $model_{intra}$ for identification of Ki-67 status in the training and testing cohort(Fig. 4B); AUC value of different ML algorithms based on $model_{peri}$ for identification of Ki-67 status in the training and testing cohort(Fig. 4C).

The predictive performance of different ML algorithms based on $model_{intra+peri}$ was summarized in Table 3. The ML classifiers for Logistic Regression and Linear Discriminant Analysis exhibited a clear superiority, with AUC scores of 0.98 (CI: 0.942, 0.986) and 0.97 (CI: 0.826, 0.989), accuracy rates of 0.98 and 0.96, sensitivities of 0.98 and 0.96, and specificities of 0.97 and 0.97 within the training cohort. In the validation cohort, they attained AUCs of 0.92 (CI: 0.955, 1.000) and 0.98 (CI: 0.674, 0.968), accuracy rates of 0.94 and 0.97, sensitivities of 1.00 and 0.96, and specificities of 0.85 and 1.00, respectively. The ROC curves in training and validation set were shown in Fig. 5. ROC curves of ML algorithms for identification of Ki-67 status in the training cohort (Fig. 5A); ROC curves of ML algorithms for identification of Ki-67 status in the validation cohort (Fig. 5B).

Discussion

In this study, we developed and validated radiomics models using 11 ML algorithms for preoperative prediction of Ki-67 expression status in BC. Radiomics features were extracted from intra- and peritumoral regions based on multi-parametric MR maps. Results showed that the combined intra- and peritumoral radiomics with ML exhibits significant predictive power for Ki-67 expression levels.

It's reported that Ki-67 plays a role in the cellular proliferation process and contributes to the heterogeneity of tumor growth kinetics [18, 23]. Several studies proved that radiomics and nomograms possess potential in Ki-67 status prediction in patients with lung adenocarcinoma or medulloblastoma [24, 25]. However, Ki-67 exists with proliferation differing from 1 to 90% in different intratumoral regions [23]. Therefore, it is necessary to evaluate the whole lesion in vivo. Among the 35 selected features from combined intra and peritumoral regions, the majority features were Gabor wavelet features, capable of providing a comprehensive quantification of tumor heterogeneity across various spatial scales and directional orientations. Recent studies [17, 18] have also indicated that Gabor wavelet features offer more detailed insights into breast cancer and are essential elements in the construction of a radiomics model.

Liang et al. [26] proposed that radiomics signatures from T2WI images were confirmed to be in accordance with the Ki-67 expression level. Yasemin et al. [18] focused on features from DCE and ADC maps to detect the Ki-67 expression level of breast cancer. However, prior radiomics studies mostly focused on single or two combined MR sequences. Huang et al. [27] suggested

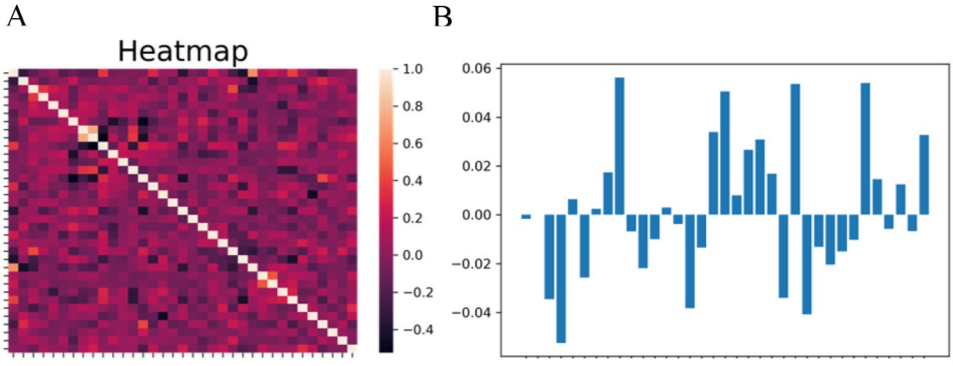

Fig. 3 Pearson correlation heatmap of selected features on predicting Ki-67 status. Dark colour denotes a positive correlation, and light colour denotes a negative correlation, and the shade of the color indicates the correlation degree (**A**).The correlation coefficients of 35 selected feature-based T2WI, DCE-T1, DWI and ADC sequences (**B**)

Table 2 Results of the feature selection for the combined intra and peritumoral radiomics model based on DCE, T2WI, DWI, ADC

Sequences	Features		Coefficients
DCE	Peritumoral Features	Original Gldm Small Dependence Low Gray Level Emphasis	0.002360951
		Wavelet-LLH First order Kurtosis	0.01730243
		Wavelet-LLH Glcmldn	0.05626885
		Wavelet-LHL Gldm Small Dependence Low Gray Level Emphasis	-0.00687314
		Wavelet-HLH Gldm Dependence Variance	-0.02193275
		Wavelet-HHL First order Mean	-0.00995817
		Wavelet-HHH First order Skewness	0.002915816
		Wavelet-LLL First order Minimum	-0.00377387
	Intratumoral Features	Wavelet-LHL Glcm Cluster Shade	-0.01505743
		Wavelet-LHH First order Skewness	-0.01023311
T2WI	Peritumoral Features	Wavelet-LLH First order Kurtosis	-0.03460180
		Wavelet-LLH Glcm MCC	-0.05261036
		Wavelet-LHH First order Skewness	0.00643968
		Wavelet-HHH Gldm Small Dependence High Gray Level Emphasis	-0.02574802
	Intratumoral Features	Original Glcm Idn	0.05052320
		Wavelet-LHL Glcm Cluster Shade	0.00797365
		Wavelet-HLL Glcm Imc1	0.02661667
		Wavelet-HLL Glszm Small Area Low Gray Level Emphasis	0.03090267
		Wavelet-HLH Glcm Inverse Variance	0.01687358
DWI	Peritumoral Features	Wavelet-LHL Ngtdm Contrast	-0.00164859
		Wavelet-LLL Glcm Imc1	3.67152E-08
	Intratumoral Features	Original First order Kurtosis	-0.03400322
		Original Glcm Imc2	0.05353916
		Wavelet-LHL Ngtdm Contrast	-0.04085949
		Wavelet-HHL Glszm Size Zone Non Uniformity Normalized	-0.01320199
		Wavelet-HHH Glszm Size Zone Non Uniformity Normalized	-0.02049154
ADC	Peritumoral Features	Wavelet-LHH Glszm Large Area Low Gray Level Emphasis	-0.03826035
		Wavelet-HLH First order Mean	-0.01349872
		Wavelet-HHL Glcm Cluster Shade	0.03386282
	Intratumoral Features	Original Firs torder 10 Percentile	0.05392699
		Wavelet-HLH First order Mean	0.01455839
		Wavelet-HLH Glcm Cluster Prominence	-0.00571082
		Wavelet-HLH Glcm Correlation	0.01249993
		Wavelet-HHH First order Skewness	-0.00676369
		Wavelet-LLL Ngtdm Busyness	0.03270688

Magnitude of the weight if their corresponding characteristics in the regression model. DCE, dynamic contrast-enhanced; T2WI, T2 weighted image; DWI, diffusion weighted image; ADC, apparent diffusion coefficient

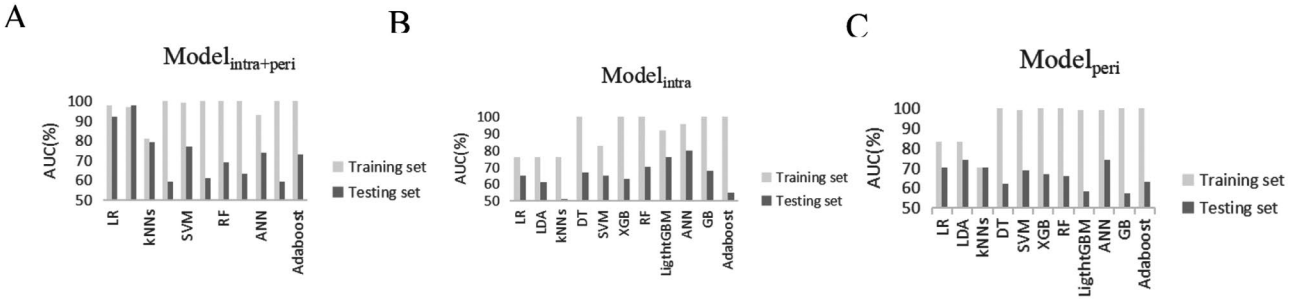

Fig. 4 The bar chart shows the analysis results of the ROC curves for different ML algorithms based on three models. AUC value of different ML algorithms based on model$_{intra+peri}$ for identification of Ki-67 status in the training and testing cohort (**A**). AUC value of different ML algorithms based on model$_{intrai}$ for identification of Ki-67 status in the training and testing cohort (**B**). AUC value of different ML algorithms based on model$_{peri}$ for identification of Ki-67 status in the training and testing cohort (**C**)

Table 3 A performance summary of ML algorithms with combined radiomics for prediction of Ki-67 status in each cohort

ML		AUC (95%CI)	ACC	SEN	SPE	PPV	NPV	F-1 score
LR	Training	0.98 (0.942, 0.986)	0.98	0.98	0.97	0.98	0.97	0.98
	Validation	0.92 (0.955, 1.000)	0.94	1.00	0.85	0.92	1.00	0.96
LDA	Training	0.97 (0.826, 0.989)	0.96	0.96	0.97	0.98	0.94	0.97
	Validation	0.98 (0.674, 0.968)	0.97	0.96	1.00	1.00	0.93	0.98
kNNs	Training	0.81 (0.764, 0.903)	0.82	0.88	0.74	0.83	0.81	0.85
	Validation	0.79 (0.675, 0.970)	0.83	0.96	0.62	0.81	0.89	0.88
DT	Training	1.00 (0.772, 0.914)	1.00	1.00	1.00	1.00	1.00	1.00
	Validation	0.59 (0.433, 0.743)	0.69	0.96	0.23	0.69	0.75	0.80
SVM	Training	0.99 (0.952, 0.995)	0.99	1.00	0.97	0.98	1.00	0.99
	Validation	0.77 (0.909, 0.993)	0.83	1.00	0.54	0.79	1.00	0.88
XGB	Training	1.00 (0.902, 0.990)	1.00	1.00	1.00	1.00	1.00	1.00
	Validation	0.61 (0.634, 0.930)	0.69	0.91	0.31	0.70	0.67	0.79
RF	Training	1.00 (0.915, 0.983)	1.00	1.00	1.00	1.00	1.00	1.00
	Validation	0.69 (0.659, 0.907)	0.75	0.91	0.46	0.75	0.75	0.82
LigthtGBM	Training	1.00 (0.907, 0.988)	1.00	1.00	1.00	1.00	1.00	1.00
	Validation	0.63 (0.647, 0.905)	0.72	0.96	0.31	0.71	0.80	0.81
ANN	Training	0.93 (0.864, 0.966)	0.92	0.86	1.00	1.00	0.83	0.92
	Validation	0.74 (0.682, 0.970)	0.78	0.87	0.62	0.80	0.73	0.83
GB	Training	1.00 (0.890, 0.984)	1.00	1.00	1.00	1.00	1.00	1.00
	Validation	0.59 (0.537, 0.903)	0.69	0.96	0.23	0.69	0.75	0.80
Adaboost	Training	1.00 (0.886, 0.980)	1.00	1.00	1.00	1.00	1.00	1.00
	Validation	0.73 (0.566, 0.870)	0.81	1.00	0.46	0.77	1.00	0.877

LR, Logistic Regression; LDA, Linear Discriminant Analysis; kNNs, k-Nearest Neighbor; SVM, Support Vector Machine; DT, Decision Tree; XGBoost, Extreme gradient boosting; RF, Random Forest; LightGBM, Light gradient boosting machine; ANN, Artificial Neural Network; GBM, Gradient boosting machine; AdaBoost, Adaptive Boosting

AUC, the area under curve; ACC, accuracy; SEN, sensitivity; SPE, specificity; NPV, negative predictive value; PPV, positive predictive value; ML, machine learning.CI: confidence interval

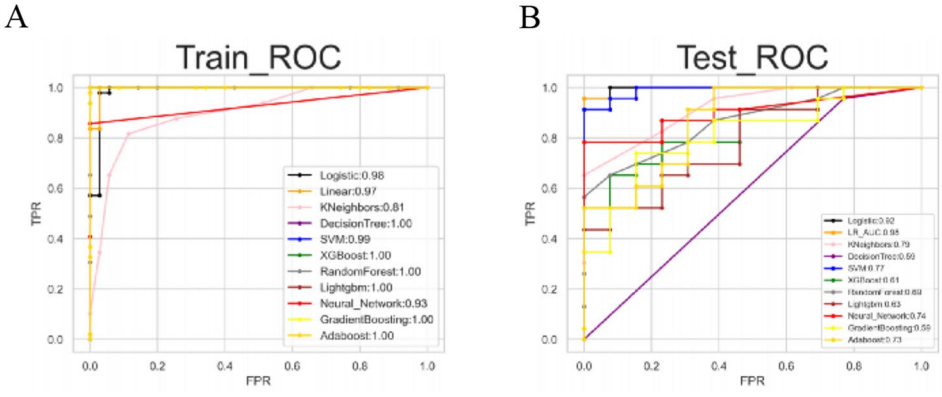

Fig. 5 Receiver operating characteristic (ROC) curves of the 11 machine learning (ML) algorithms with combined radiomics for identification of Ki-67 status in the training and validation cohorts. ROC curves of ML algorithms for identification of Ki-67 status in the training cohort (**A**); ROC curves of ML algorithms for identification of Ki-67 status in the validation cohort (**B**). FPR, False Positive Rate; TPR, True Positive Rate

that radiomics based on multi-parametric MRI maps combining with ML approaches can predict the molecular subtype and expression of AR in BC non-invasively. A recent study by Mayidili et al. [15] proposed that ADC maps achieve a better predictive efficacy for lymphovascular invasion (LVI) than two or three combinations of MR sequences in patients with invasive breast cancer. The result was inconsistent with our study that the fusion radiomics features based on multi parametric MRI achieved good AUC in predicting Ki-67 expression level. The role of the fusion radiomics model needs to be tested in larger datasets.

With the development of computer science, ML, as a branch, becomes the emerging technology which can learn patterns from data to improve performance at different tasks [28, 29]. Gigi et al. [30] reported that personal health data and ML models, including neural network models have better predictive accuracy for breast cancer

risk compared with the Breast Cancer Risk Prediction Tool (BCRAT). We developed and compared various ML algorithms based on 14, 23 and 35 features selected from intratumor, peritumor, and combined intratumor+peritumor ROIs. Among the three models, all algorithms achieved a high AUC value on the training set, yet only the LR and LDA algorithms of $Model_{intra+peri}$ reached an impressive 0.92 and 0.98 in the testing set, indicating a high level of predictive efficacy. In contrast, the AUC values for the algorithms in $Model_{intra}$ and $Model_{peri}$ were consistently below 0.8 in the testing set, suggesting that these models suffered from over fitting, which consequently led to insufficient predictive performance.

Logistic Regression is an algorithm that employs the logistic function to estimate probabilities, making it particularly effective for handling high-dimensional datasets. This method excels in scenarios where the datasets can be linearly separated [31]. On the other hand, Linear Discriminant Analysis is closely related to regression and variance analysis. In this context, the dependent variable can be understood as a linear combination of other characteristics or measured values [31]. When applied in the field of radiomics models, both LR and LDA algorithms demonstrate significant potential in prediction tasks. This is primarily due to their robust capabilities in processing high-throughput data, allowing for the accurate estimation of probabilities and the interpretation of dependent variables in terms of linear combinations of other features.

In the comparing study, the AUC values for the algorithms in $model_{intra}$ or $model_{peri}$ were consistently below 0.8 in the testing set, but algorithms of $Model_{intra+peri}$ achieved high AUC values, suggesting that combined intra and peritumoral radiomics can provide more detailed information about the tumor. Prior studies based on radiomics mainly focused on features from intratumoral regions. However, the tumor heterogeneity was consisted of intratumoral and peritumoral heterogeneity [32]. Features of the micro-environment around the tumor were related to peritumoral edema and blood vessel invasionare, which were connected with cancer progression and metastasis [33]. Niu et al. [34] found that features from the peritumoral regions at a 2 mm peritumoral size achieved the best discriminative performance in the differentiation of benign and malignant breast lesions. Zhang et al. [21] suggested that a 6 mm dilation distance was suitable for classification tasks for hormone receptor (HR) and an 8 mm dilation distance suitable for HER2. Thus, the dilation distance varies in MR-reported researches, and there is no accurate criterion. In our study, we chose a 5.0 mm dilation distance, which was in accordance with the investigation of Braman et al. [35], who reported that the peri- and intratumoral DCE-MRI imaging features with 2.5 mm to 5.0 mm dilation distances obtained great ability in predicting pCR after receiving NAC in patients with BC.

Limitations

There were some limitations in our study. Firstly, as a retrospective study, the patient volume was relatively small from a single center. To improve the predictive efficiency, it is requested for a larger multi-center study. Secondly, based on DCE-MRI maps, this study extracted features from the second-phase images, further information would be ignored without integration of multi-phase images. Thirdly, the tumor circumference was obtained by expanding outward at a distance of 5 mm, there is no evidence whether it is the optimal peritumoral range. Fourthly, inter or intra-reader variability measures should be utilized to assess the inter or intraobserver agreement in image annotation, as this constitutes a limitation of the study. Fifthly, this article omits a comparative analysis of single-sequence MR versus multi-sequence MR, meriting further investigation.

Conclusion

We developed and validated a radiomics machine learning model for the preoperative prediction of Ki-67 expression status, which is based on combined intra- and peritumoral features derived from multi-parameter MR maps. This predictive model offers individualized guidance for patients with BC, both before and after therapy, by forecasting the expression status of Ki-67 in a timely and noninvasive manner.

Supplementary Information

The online version contains supplementary material available at https://doi.org/10.1186/s12880-025-01553-z.

Supplementary Material 1

Acknowledgements

Not applicable.

Author contributions

Guarantor of integrity of the entire study: Ning Ding. Study concepts and design: Yan Lu. Literature research: Yan Lu, Mengjuan Li, Shengnan Yin. Clinical studies: Yan Lu, Mengjuan Li. Experimental studies / data analysis: Yan Lu, Yiding Ji, Shengnan Yin. Statistical analysis: Ning Ding, Yiding Ji. Manuscript preparation: Yan Lu. Manuscript editing: Yan Lu, Long Jin, Ning Ding.

Funding

This study is supported by a grant from Science and Technology Development Program of Suzhou (grant: SKYD2023240), and Academic Project of Suzhou Ninth hospital (grant: YK202336).

Data availability

The data that support the findings of this study are available from the corresponding author, upon reasonable request.

Declarations

Ethics approval and consent to participate
This study was approved by the Ethics Committee of the Suzhou Ninth People'sHospital(registration number: KY2023-040-01). The requirement for indi-vidual informed consentwas waived by the committee (full name: The Ethics Committee of the Suzhou Ninth People'sHospital) because of the retrospective nature of the study. The data are anonymous, and therequirement for informed consent was therefore waived.

Consent for publication
Not applicable.

Competing interests
The authors declare no competing interests.

Author details
[1]Department of Radiology, Suzhou Ninth People's Hospital, Ludang Street 2666#, Suzhou, Jiangsu 215200, PR China

Received: 25 April 2024 / Accepted: 3 January 2025
Published online: 07 January 2025

References

1. Fidler MM, Soerjomataram Guptas. Cancer incidence and mortality among young adults aged 20–39 years worldwide in 2012: a population-based study. Lancet Oncol. 2017;18(12):1579–89.
2. Sung H, Ferlay J, Siegel RL, et al. Global Cancer statistics 2020: Globocan estimates of incidence and Mortality Worldwide for 36 cancers in 185 countries. CA Cancer J Clin. 2021;71(3):209–49.
3. DE Azambuja E, Cardoso F, DE Castro G JR, et al. Ki-67 as prognostic marker in early breast cancer: a meta-analysis of published studies involving 12,155 patients. Br J Cancer. 2007;96(10):1504–13.
4. Yerushalmi R, Woods R, Ravdin P M, et al. Ki67 in breast cancer: prognostic and predictive potential. Lancet Oncol. 2010;11(2):174–83.
5. Ignatiadis M, Azim H A JR. The genomic Grade Assay compared with Ki67 to determine risk of distant breast Cancer recurrence. JAMA Oncol. 2016;2(2):217–24.
6. Ragab H M, Samy N, Afify M, et al. Assessment of Ki-67 as a potential biomarker in patients with breast cancer. Genet Eng Biotechnol. 2018;16(2):479–84.
7. Diwakar N, Sperandio M, Sherriff M, et al. Heterogeneity, histological features and DNA ploidy in oral carcinoma by image-based analysis. Oral Oncol. 2005;41(4):416–22.
8. Chen X, HE C, Han D, et al. The predictive value of Ki-67 before neoadjuvant chemotherapy for breast cancer: a systematic review and meta-analysis. Future Oncol. 2017;13(9):843–57.
9. Ellis MJ, Suman V J, Hoog J, et al. Ki67 Proliferation Index as a Tool for Chemotherapy decisions during and after neoadjuvant aromatase inhibitor treatment of breast Cancer: results from the American College of Surgeons Oncology Group Z1031 Trial (Alliance). Clin Oncol. 2017;35(10):1061–9.
10. Dowsett M, Smith I E, Ebbs S R, et al. Prognostic value of Ki67 expression after short-term presurgical endocrine therapy for primary breast cancer. Natl Cancer Inst. 2007;99(2):167–70.
11. Bera K, Braman N, Gupta A, et al. Predicting cancer outcomes with radiomics and artificial intelligence in radiology. Nat Rev Clin Oncol. 2022;19(2):132–46.
12. Rizzo S, Botta F, Raimondi S, et al. Radiomics: the facts and the challenges of image analysis. Eur Radiol Exp. 2018;2(1):36.
13. Guiot J, Vaidyanathan A, Deprez L, et al. A review in radiomics: making personalized medicine a reality via routine imaging. Med Res Rev. 2022;42(1):426–40.
14. Zhang J, Wang G, Ren J, et al. Multiparametric MRI-based radiomics nomogram for preoperative prediction of lymphovascular invasion and clinical outcomes in patients with breast invasive ductal carcinoma. Eur Radiol. 2022;32(6):4079–89.
15. Nijiati M, Aihaiti D, Huojia A, et al. MRI-Based Radiomics for Preoperative Prediction of Lymphovascular Invasion in patients with invasive breast Cancer. Front Oncol. 2022;12:876624.
16. Yuan C, Jin F, Guo X, et al. Correlation analysis of breast Cancer DWI combined with DCE-MRI Imaging features with molecular subtypes and prognostic factors. Med Syst. 2019;43(4):83.
17. LI C, Song L. Intratumoral and Peritumoral Radiomics based on functional Parametric maps from breast DCE-MRI for prediction of HER-2 and Ki-67 status. Magn Reson Imaging. 2021;54(3):703–14.
18. Kayadibi Y, Kocak B, Ucar N, et al. Radioproteomics in breast Cancer: prediction of Ki-67 expression with MRI-based Radiomic models. Acad Radiol. 2022;29(Suppl 1):S116–25.
19. Cui H, Zhang D, Peng F, et al. Identifying ultrasound features of positive expression of Ki67 and P53 in breast cancer using radiomics. J Asia Pac J Clin Oncol. 2021;17(5):e176–84.
20. Liu W, Cheng Y, Liu Z, et al. Preoperative prediction of Ki-67 status in breast Cancer with multiparametric MRI using transfer learning. Acad Radiol. 2021;28(2):e44–53.
21. Zhang S, Wang X, Yang Z, et al. Intra- and Peritumoral Radiomics Model based on early DCE-MRI for Preoperative Prediction of Molecular subtypes in Invasive Ductal breast carcinoma: a Multitask Machine Learning Study. Front Oncol. 2022;12:905551.
22. Liu Y, Li X, Zhu L, et al. Preoperative prediction of Axillary Lymph Node Metastasis in breast Cancer based on Intratumoral and Peritumoral DCE-MRI Radiomics Nomogram. Contrast Media Mol Imaging. 2022;2022:6729473.
23. Porschen R, Lohe B, Hengels K J, et al. Assessment of cell proliferation in colorectal carcinomas using the monoclonal antibody Ki-67. Correlation with pathohistologic criteria and influence of irradiation. Cancer. 1989;64(12):2501–5.
24. Yan J, Xue X, Gao C, et al. Predicting the Ki-67 proliferation index in pulmonary adenocarcinoma patients presenting with subsolid nodules: construction of a nomogram based on CT images. Quant Imaging Med Surg. 2022;12(1):642–52.
25. Zhou L, Peng H, JI Q, et al. Radiomic signatures based on multiparametric MR images for predicting Ki-67 index expression in medulloblastoma. Ann Transl Med. 2021;9(22):1665.
26. Liang C, Cheng Z, Huang Y, et al. An MRI-based Radiomics Classifier for Preoperative Prediction of Ki-67 status in breast Cancer. Acad Radiol. 2018;25(9):1111–7.
27. Huang Y, Wei L, Hu Y, et al. Multi-parametric MRI-Based Radiomics models for Predicting Molecular Subtype and Androgen receptor expression in breast Cancer. Front Oncol. 2021;11:706733.
28. Bzdok D, Krzywinski M, Altman N. Machine learning: supervised methods. Nat Methods. 2018;15(1):5–6.
29. Kourou K, Exarchos T P, Exarchos K P, et al. Machine learning applications in cancer prognosis and prediction. Comput Struct Biotechnol J. 2015;13:8–17.
30. Stark G F, Hart G R, Nartowt B J, et al. Predicting breast cancer risk using personal health data and machine learning models. PLoS ONE. 2019;14(12):e0226765.
31. Sarker I H. Machine learning: algorithms, real-world applications and research directions. SN Comput Sci. 2021;2(3):160.
32. Semenza G L. The hypoxic tumor microenvironment: a driving force for breast cancer progression. Biochim Biophys Acta. 2016;1863(3):382–91.
33. Jia JB, Wang W Q, Sun H C, et al. High expression of macrophage colony-stimulating factor-1 receptor in peritumoral liver tissue is associated with poor outcome in hepatocellular carcinoma after curative resection. Oncologist. 2010;15(7):732–43.
34. Niu S, YU T, Cao Y, et al. Digital breast tomosynthesis-based peritumoral radiomics approaches in the differentiation of benign and malignant breast lesions. Diagn Interv Radiol. 2022;28(3):217–25.
35. Braman N, Prasanna P, Whitney J, et al. Association of Peritumoral Radiomics with Tumor Biology and pathologic response to Preoperative targeted therapy for HER2 (ERBB2)-Positive breast Cancer. JAMA Netw Open. 2019;2(4):e192561.

Publisher's note